Available online at www.sciencedirect.com

SCIENCE DIRECT®

Cement and Concrete Research 35 (2005) 1764–1775

Cement and Concrete Research

Effects of porosity on leaching of Ca from hardened ordinary Portland cement paste

Kazuko Haga[a,*], Shunkichi Sutou[a], Michihiko Hironaga[b], Satoru Tanaka[c], Shinya Nagasaki[d]

[a]*Taiheiyo Consultant Co. Ltd., 2-4-2, Osaku, Sakura-City, Chiba 285-8655, Japan*
[b]*Central Research Institute of Electric Power Industry, 1646, Abiko, Abiko-City, Chiba 270-1194, Japan*
[c]*Department of Quantum Engineering and Systems Sciences, University of Tokyo, 7-3-1, Hongo, Bunkyo-ku, Tokyo 113-8656, Japan*
[d]*Institute of Environmental Studies, Graduate School of Frontier Sciences, University of Tokyo, 7-3-1, Hongo, Bunkyo-ku, Tokyo 113-8656, Japan*

Received 9 October 2003; accepted 21 June 2004

Abstract

Aiming at evaluating the effects of porosity in hardened cement paste on dissolution phenomena, we prepared hardened ordinary Portland cement (OPC), with variation in pore volume, and then leached them in deionized water. It was found that the bulk density and pore volume were affected by the dissolution of portlandite. The larger the pore volume of the sample, the more rapidly portlandite is dissolved. An electron probe microanalysis (EPMA) performed on the cross-section of the solid phase showed the 'portlandite (CH) dissolution front'. As the leaching period became longer, the CH dissolution front shifted towards the inner part. In addition, the movement of the CH dissolution front was described by the diffusion model, with consideration of the dissolution of portlandite. It was concluded that the transport of leached constituents is diffusion controlled, and the major leached constituents of hardened OPC are portlandite and C-S-H gel. Large pore, which was generated associated with the leaching of portlandite, was considered significantly to affect the diffusion of leached constituents.

Keywords: Degradation; Diffusion; Calcium-silicate-hydrate; Pore size distribution; Long-term performance

1. Introduction

The alteration of cement paste due to dissolution is assumed to rarely become an issue for concrete structures used in general use. However, it is a very important phenomena for concrete structures used in radioactive waste disposal facilities, on which long-term performance assessment is required, and an understanding of the dissolution phenomena is considered to be one of the very important technical subjects [1]. Cementitious materials have been used as structural or filling materials in radioactive waste disposal facilities. However, the long-term alteration of cement paste, in terms of its mechanical strength and chemical properties, is far from being completely understood, leaving uncertainty in the predictions of the long-term safety performance of the disposal facilities. In disposal facilities to be constructed in the underground, cementitious materials would be dissolved and altered by contact with groundwater. This dissolution-induced alteration is considered to be one of the major factors that alter the physical properties of concrete structures.

The dissolution-induced alteration is considered to consist of the leaching of cement constituents into the pore water and the transportation of leached constituents. Many studies have been reported on the leaching of cement constituents from cement hydrate. Change of chemical properties (pH, concentration of constituent, etc.) of pore water by leaching of hardened cement paste has been intensively studied because it is assumed to affect the transportation of radioactive nuclides and surrounding environmental chemistry in the repository. Atkinson et al. [2,3], Atkinson and Guppy [4] and Berner [5] developed cement paste dissolution models to evaluate long-term change in the composition of liquid phase. Faucon et al.

* Corresponding author. Tel.: +81 43 498 3858; fax: +81 43 498 3859.
E-mail address: Kazuko_Haga@grp.taiheiyo-cement.co.jp (K. Haga).

0008-8846/$ - see front matter © 2004 Elsevier Ltd. All rights reserved.
doi:10.1016/j.cemconres.2004.06.034

Table 1
Chemical composition of ordinary Portland cement (wt.%)

SiO_2	Al_2O_3	Fe_2O_3	CaO	MgO	SO_3	Na_2O	K_2O
20.55	5.26	2.73	64.26	1.18	1.98	0.29	0.36

[6,7] studied the alteration of hardened cement paste by dissolution and indicated that hydrate phases and structure of hydrates would change with the progress of dissolution.

Meanwhile, Buil [8], Carde et al. [9], Adenot [10] and Yokozeki [11] considered diffusion as the transport mechanism of leached constituents in their models. Buil [8] modeled alteration due to the leaching and diffusion of Ca from hardened cement paste to analyze the distribution of Ca concentration in the hardened cement paste with time. Yokozeki [11] also developed a similar model to evaluate the dissolution phenomena of concrete structure contacted with water for a long period. Toyohara et al. [12] modeled the leaching and transportation of leached constituents by water flow (advection) and compared the analysis with experimental results.

However, studies focused on the structural change of hardened cement paste associated with dissolution have been hardly reported. Considering that the change in the hardened cement paste with the progress of dissolution is an important issue to be clarified for the evaluation of physical and chemical durability, as well as modeling of cement paste alteration, we have performed leaching tests of cement hydrates to evaluate the change in structures of hydrates and pores [13–15]. We have reported that the silicate anion chains of the C-S-H gel were elongated in the samples after leaching and that the structure of hydrates would change as a result of dissolution [13,16]. It was also indicated that the change in the pore structure of hardened cement paste is correlated with the leaching hydrate: The leaching of a major hydrate, portrandite, would increase the volume of larger pores, and C-S-H gel and ettringite would be generated simultaneously after leaching [15,17]. Such leaching phenomena progresses as follows. First, the cement constituents leach into the pore water of the hardened cement paste. Then, the leached constituents diffuse in the pore by the concentration gradient, and therefore, the pore volume of the hardened cement paste was considered to affect the dissolution phenomena.

In the present study, aiming at evaluating the effects of pore volume in hardened cement paste on dissolution phenomena, we prepared hardened cement paste with variation in pore volume and then conducted leaching test for them in deionized water for a predetermined period. Analyzing the alteration of hardened cement paste after leaching in detail, we discussed the effects of pore volume on the progress of dissolution. And with a mass balance equation for one dimensional diffusion as a basic formula, dissolution phenomena of hardened cement paste was evaluated using a conventional model that takes into account the leaching of C-S-H gel and increase of pore volume due to the leaching of portlandite. The weight ratio of deionized water to the sample in the leaching tests was kept constant at 1000, which was for observing the dissolution phenomena in a short time, although it is quite different from real underground conditions, where a reaction would be expected to progress much more slowly than this experiment.

2. Experiments

2.1. Test samples

Ordinary Portland cement (OPC) was mixed with deionized water at water-to-cement weight ratios (W/C ratio) of 0.4, 0.6, 0.8 and 1.0. The chemical compositions of the OPC used in the tests are shown in the Table 1. As the cement paste with higher W/C ratio results in bleeding (separation of water) at the top of the paste, in general, by which porosity, as well as the W/C ratio, in the hardened body becomes smaller, samples at W/C ratios of 0.6, 0.8 and 1.0 were repeatedly mixed before setting to prevent bleeding and to form hydrated texture with relatively large porosity, where pores are homogeneously distributed in the samples. Curing was for 56 days at 50 °C underwater. The characteristics of the prepared hardened OPC are shown in Table 2. The porosities of the hardened samples were varied in the range of 22–58% [mercury intrusion porosimetry (MIP)], depending on the W/C ratio. Small quantities of nonhydrated minerals were identified in the samples by X-ray diffraction (XRD) analysis. Hardened OPC after curing were cut and shaped to plates of 2.5×10×10 mm using a diamond cutter, for use as specimens in the dissolution tests.

2.2. Dissolution tests

The hardened OPC were sealed in polyethylene containers with deionized water at the liquid-to-solid-weight ratio of 1000 and were left in a thermostatic chamber at 20 °C for a predetermined period (1, 3, 5, 7, 28, 56 and 91 days). The leaching water was not exchanged. After a specified period, solid and leaching water were separated by decantation. The solid samples were dried in a vacuum dryer. The entire process, from the leaching of samples through the vacuum drying, was conducted in a controlled atmosphere in a glove box, where air was replaced with N_2 gas (Table 3).

Table 2
Porosity and hydrated phase

Porosity	W/C	0.4	0.6	0.8	1.0
	Porosity (%)	21.5	39.5	51.6	57.7
Hydrate phase	Portlandite, C-S-H gel, AFm, calcite, alite, belite and ferrite phase				

Table 3
Experimental conditions

Samples for leaching	OPC hydrate 2.5×10×10 mm (under sealed condition for 56 days at 50 °C) decarbonated ion exchanged water (purged by Ar gas for 24 h)
Liquid/solid ratio for leaching	1000 (wt./wt.)
Leaching period	1, 3, 5, 7, 28, 56 and 91 days
Condition of dissolution test	In the glove box filled with argon gas

2.3. Analysis method

The pH of the aqueous sample was measured using a glass electrode (Horiba, B-211) in a glove box. After the measurement of pH, the aqueous sample was taken out from the glove box. Then, it was changed to acidic solution with HCl immediately. Ca concentration in the aqueous sample was measured using an inductively coupled plasma emission spectrometer (ICP; Varian, VISTA-AX).

After being vacuum dried, the solid-phase samples were subjected to measurement of pore size distribution, bulk density, etc., using MIP (Micrometrics, Type: Auto pore II 9220). Some sample pieces were embedded in resin, cut through the center and polished for element concentration analyses using electron probe microanalysis (EPMA; JEOL JXA-8621). The other sample pieces were prepared for XRD analyses (Rigaku, RINT2050) to identify the crystal phases and for differential thermal analysis and thermogravimetry (DTA/TG; Seiko Instruments, SSC5000).

3. Results and discussion

3.1. Relationship between the leaching period and the composition of the aqueous phase

The relationships between the leaching period and the pH and the concentration of Ca of the aqueous sample are shown in Fig. 1. The pH and the concentration of Ca for the samples with W/C of 0.8 and 1.0 increased as the leaching period was extended; then, at 56 days, the pH became 12.2, and Ca concentration became 6×10^{-3} mol/l. The pH and the concentration of Ca showed a tendency to converge into a constant value for 56 days, which indicated that the aqueous and solid phases were in an equilibrium state.

However, the pH and the Ca concentration of the aqueous phase for the samples with W/C 0.4 and 0.6 continued to change as the leaching period was extended; these did not converge into constant values. The aqueous and solid phases of these samples were not in an equilibrium state in 91 days, which suggests that the leaching was continued.

3.2. Changes in the hydrate phase

The crystal phases identified by XRD are shown in Table 4. In the initial samples, hydrate phases of portlandite, C-S-H gel and ettringite ($3CaO\cdot Al_2O_3\cdot 3CaSO_4\cdot 32H_2O$) and the AFm phase (monosulfate phase: $3CaO\cdot Al_2O_3\cdot CaSO_4\cdot 12H_2O$; monocarbonate phase: $3CaO\cdot Al_2O_3\cdot CaCO_3\cdot 12H_2O$; hemicarbonate phase: $7CaO\cdot 2Al_2O_3\cdot CaCO_3\cdot 24H_2O$) were observed. Calcite was also observed, which could have been formed partly by carbonization during the preparation of the samples. Moreover, alite ($3CaO\cdot SiO_2$), belite ($2CaO\cdot SiO_2$) and ferrite phase ($4CaO\cdot Al_2O_3\cdot Fe_2O_3$) as unhydrated clinker minerals were observed.

The relationship between the leaching period and the strength of the diffraction peak of portlandite normalized to that of the initial samples is shown in Fig. 2. The strength of the diffraction peaks are dependent on W/C, therefore, they normalized to the initial sample. The peak strength of the portlandite became smaller as the samples were leached for longer periods. The larger the W/C of the samples, the peak strength of portlandite became smaller rapidly. No peak was observed in the samples of W/C 0.8 and 1.0 leached for 28 days. The results of the quantitative determination of portlandite and calcite using DTA/TG are shown in Fig. 3. The amount of portlandite decreased as the leaching period

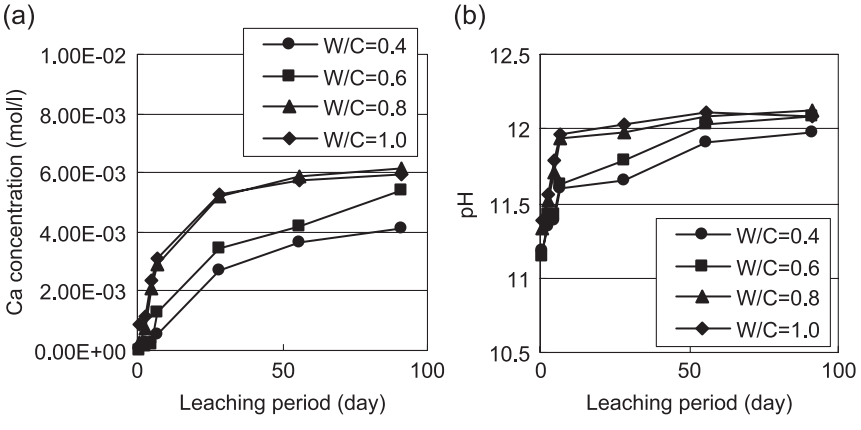

Fig. 1. Change of Ca concentration (a) and pH (b) with the leaching period.

Table 4
The crystal phase in the solid phase identified by XRD

Sample	Leaching periods	Crystal phases									
		Portlandite	C-S-H	Calcite	Ettringite	AFm	AFmCH12	AFmCH24	Alite	Belite	Ferrite phase
W/C 0.4	Initial	◎	△	○	–	△	–	–	△	△	△
	1	◎	△	○	–	△	–	–	△	△	△
	3	◎	△	○	–	△	–	–	△	△	△
	5	◎	△	○	–	△	–	–	△	△	△
	7	◎	△	○	–	△	–	–	△	△	△
	28	○	△	○	–	△	–	–	△	△	△
	56	○	△	○	△	△	–	–	△	△	△
	91	○	△	○	△	△	–	–	△	△	△
W/C 0.6	Initial	◎	△	○	–	–	△	–	△	△	△
	1	◎	△	○	–	○	△	–	△	△	△
	3	◎	△	○	△	○	△	–	△	△	△
	5	◎	△	○	–	○	△	–	△	△	△
	7	◎	△	○	△	△	△	–	△	△	△
	28	◎	△	○	△	△	△	–	△	△	△
	56	○	△	○	○	–	△	–	△	△	△
	91	△	△	○	△	–	△	–	△	△	△
W/C 0.8	Initial	◎	△	○	△	△	○	–	△	△	△
	1	◎	△	○	△	○	○	–	△	△	△
	3	◎	△	○	△	○	○	–	△	△	△
	5	◎	△	○	△	○	○	–	△	△	△
	7	◎	△	○	△	△	○	–	△	△	△
	28	–	△	○	△	–	○	–	△	△	△
	56	–	△	○	○	–	△	–	△	△	△
	91	–	△	○	○	–	△	–	△	△	△
W/C 1.0	Initial	◎	△	○	△	–	○	○	△	△	△
	1	◎	△	○	△	○	○	○	△	△	△
	3	◎	△	○	△	○	○	○	△	△	△
	5	◎	△	○	△	○	○	○	△	△	△
	7	◎	△	○	△	△	○	○	△	△	△
	28	–	△	○	△	–	△	○	△	△	△
	56	–	△	○	○	–	△	–	△	△	△
	91	–	△	○	○	–	–	–	△	△	△

XRD intensity—◎: strong (over 10,000 cps); ○: medium (1000–10,000 cps); △: weak (under 1000 cps); and –: N.D.
Portlandite: $Ca(OH)_2$; calcite: $CaCO_3$; ettringite: $3CaO \cdot Al_2O_3 \cdot 3CaSO_4 \cdot 32H_2O$; AFm: $3CaO \cdot Al_2O_3 \cdot CaSO_4 \cdot 12H_2O$; AFmCH12: $3CaO \cdot Al_2O_3 \cdot CaCO_3 \cdot 12H_2O$ AFmCH24: $7CaO \cdot 2Al_2O_3 \cdot CaCO_3 \cdot 24H_2O$; alite: $3CaO \cdot SiO_2$; belite: $2CaO \cdot SiO_2$; and ferrite phase: $4CaO \cdot Al_2O_3 \cdot Fe_2O_3$.

increased, and this result was consistent with the results obtained using XRD. The portlandite in the samples was considered to have dissolved completely during the 28 days of the test.

The relationship between the leaching period and the strength of the diffraction peak of the monosulfate phase normalized to that of the initial samples is shown in Fig. 4.

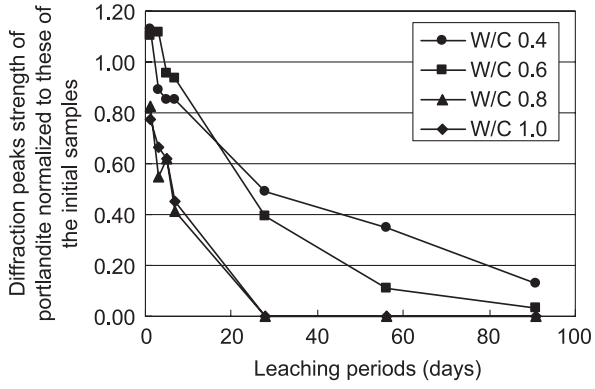

Fig. 2. The relation between the diffraction peaks strength of portlandite normalized to these of the initial samples and leaching periods.

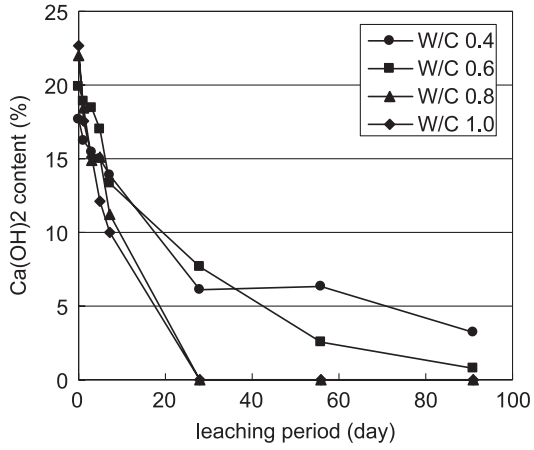

Fig. 3. Leaching time dependency of $Ca(OH)_2$ content, which was measured by DTA/TG.

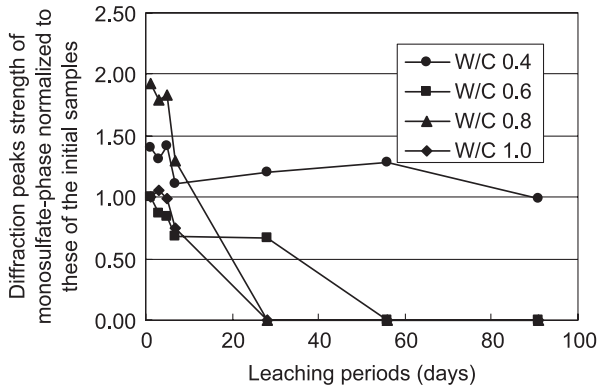

Fig. 4. The relation between the diffraction peaks strength of the monosulfate phase normalized to that of the initial samples and leaching periods.

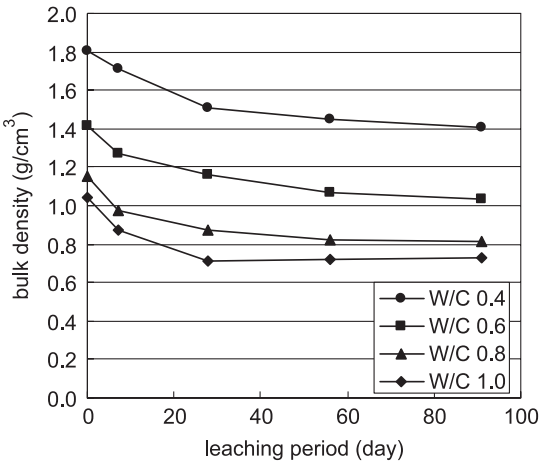

Fig. 5. Leaching time dependency of the bulk density.

The diffraction peak strength of the monosulfate phase became smaller as the samples were leached for longer periods. It became undetectable in the samples of W/C 0.8 and 1.0 leached for 28 days. The monosulfate phase in the samples was also considered to have dissolved during the 28 days of the test. The peak strength of the monosulfate phase in the samples of W/C 0.4 did not become smaller. The inside, unaltered part was observed in the samples of W/C 0.4 after being leached for 91 days, as described after. It was considered that the monosulfate phase existed in the unaltered part. In addition, Faucon et al. [18] considered that the monosulfate phase was generated in the samples after portlandite was dissolved. Therefore, it was considered that both the reaction of dissolution and generation occurred in the sample of W/C 0.4. The monocarbonate phase, which was observed in the initial samples, was still found unchanged in the samples after leaching.

In the absence of portlandite and monosulfate phase, it was observed that the diffraction peak strength of ettringite became larger. It was considered that the ettringite was generated in the samples after the portlandite and monosulfate phase were dissolved.

3.3. Changes in the pore structure

3.3.1. Changes in the bulk density

The relationship between leaching period and the bulk density is shown in Fig 5. The bulk density became smaller with the increasing leaching period. This indicates that the dissolution progressed gradually. The decrease in the bulk density of the samples with W/C 0.8 and 1.0 was relatively rapid until the 28th day. However, it remained almost unchanged after this, meaning that the weight reduction due to dissolution was mostly completed in 28 days. However, the bulk density of the samples with W/C 0.4 and 0.6 continued to change as the leaching period was extended, which suggests that the leaching was continued.

3.3.2. Changes in the pore structure

The change in the pore volume with increasing leaching period is shown in Fig. 6. The pore volume becomes larger with longer leaching periods. After 56 days, the pore volume increase rate became moderate. The relationship between the decrease of $Ca(OH)_2$ and increments of pore volume compared with the initial samples is shown in Fig. 7. It was shown that the increase of pore volume became larger with a larger decrease in the quantity of $Ca(OH)_2$. It was considered that the increases in pore volume were attributable to the dissolution of $Ca(OH)_2$, but the value scattered in the samples with high W/C.

The distributions of pore sizes measurement by MIP in the initial samples and those after leaching for 91days are shown in Fig. 8. There were many pores with the diameter of about 0.02 μm in the initial sample of W/C 0.4. There were many pores with relatively large diameter in the initial samples of W/C 0.6, 0.8 and 1.0 because these samples were made with the process of remixing before setting. As the W/C became higher, the pore diameter with maximum amount at the distribution of pore size became larger, and the amount of total pore

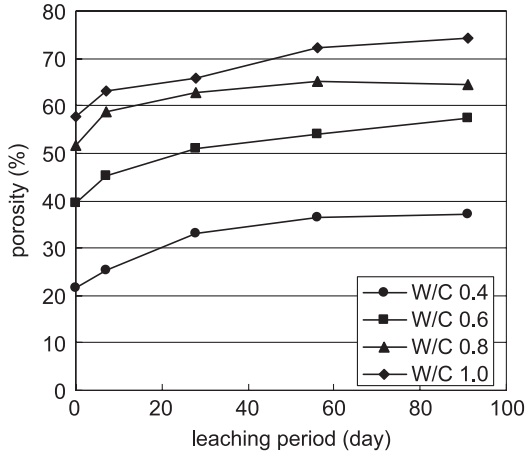

Fig. 6. Leaching time dependency of the porosity.

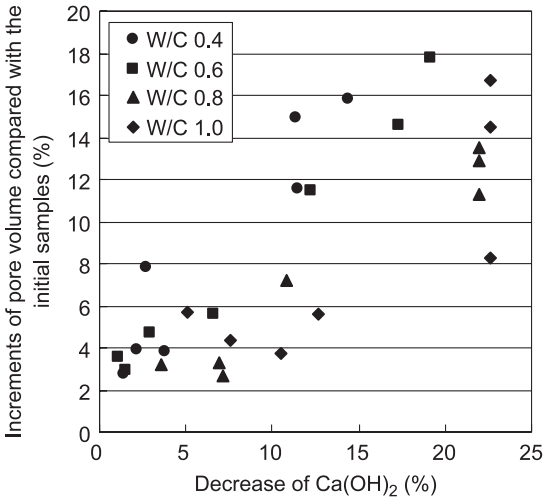

Fig. 7. $Ca(OH)_2$ decrease dependency of the increments of pore volume compared with the initial samples.

volume increased. In the leached samples of all W/C, the pores of larger diameter than the initial samples were observed, and the pores with diameter less than 0.1 μm increased. In Portland cement, the primary hydrate phases are C-S-H gel and portlandite. Each of the various hydrate phases that constitute the hardened cement paste has a different shape. In a commonly used textbook, the pores in hardened cement paste are divided into gel and capillary pores. The size of gel pores is described as being 1–3 nm in diameter, and that of capillary pores, 3 nm–30 μm. Daimon et al. [19] considered that the C-S-H gel consisted of gel particles with an internal structure, together with pores with equivalent diameters of 3.2–200 nm. These pores were termed "intergel particle pores". The smaller pores within the gel particles, termed "intercrystallite pores", had diameters of 1.2–3.2 nm. Pores smaller than these two types were termed "intracrystallite pores". The idea is not that the pores are classified into gel and capillary pores, but that the pores derived from the C-S-H gel are identified in detail. Based on this information, pores below 0.1 μm, which were increased after leaching, were considered to be related to the C-S-H gel. On the other hand, in hardened cement pastes, $Ca(OH)_2$ is often observed in the form of crystals larger than a few microns. It was assumed that the increase in the size of pores larger than it was observed in initial samples were attributable to the dissolution of $Ca(OH)_2$. It was observed that pore size distribution measured by MIP presents some problems. For example, it is reported that pore diameters determined by MIP measurement are smaller than those observed by SEM. However, portlandite in the hardened cement paste is a large crystal, and the C-S-H gel is a very small crystal in comparison. Therefore, it was believed that the change in pore size distribution caused by the dissolution of portlandite and C-S-H gel was distinguishable.

Fig. 9 shows the increase in the pore volume associated with dissolution, both values being calculated based on the measured quantity of portlandite by DTA/TG. The increase in the pore volume (V_p) resulting from

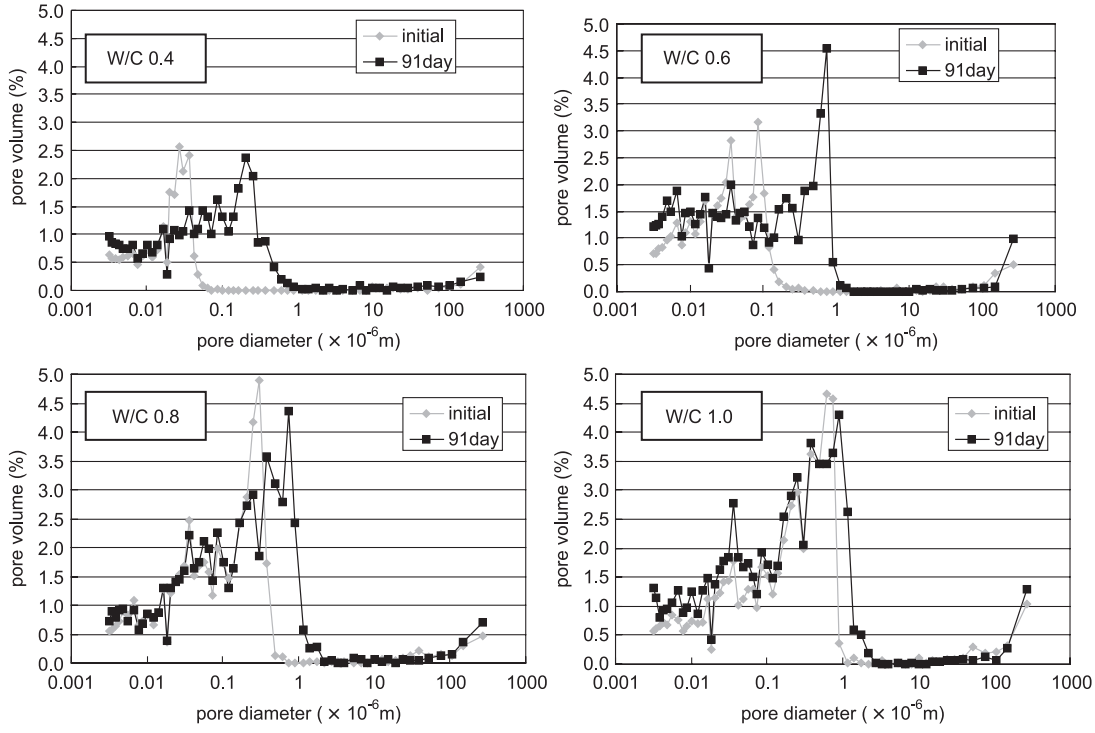

Fig. 8. Pore size distribution of the initial sample and that leached for 91 days.

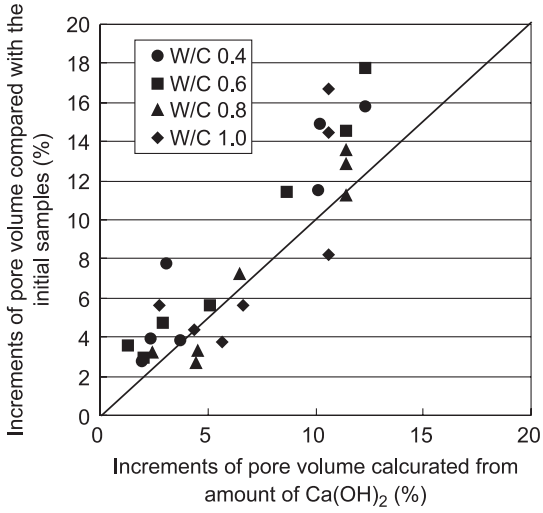

Fig. 9. Increments of pore volume associated with dissolution.

the dissolution of portlandite was calculated using the following formula

$$V_p(\%) = [(D_I \times P_I/m) - (D_L \times P_L/m)]M \times 100, \quad (1)$$

where D_I is the bulk density (g/cm^3) of the initial samples, P_I is the portlandite content by weight in the initial samples, D_L is the bulk density (g/cm^3) of the samples after leaching, P_L is the portlandite content by weight in the samples after leaching, m is the molecular weight of the portlandite (74 g/mol) and M is the molecular volume (33.0 cm^3/mol, calculated from the density of portlandite of 2.24g/cm^3, as shown in Ref. [20]). The bulk density of each sample was determined by MIP, while the portlandite content by quantitative analysis with DTA/TG. A fine agreement was found between the increments of pore volumes and those calculated from the amount of $Ca(OH)_2$. However, there were many samples that the experimental

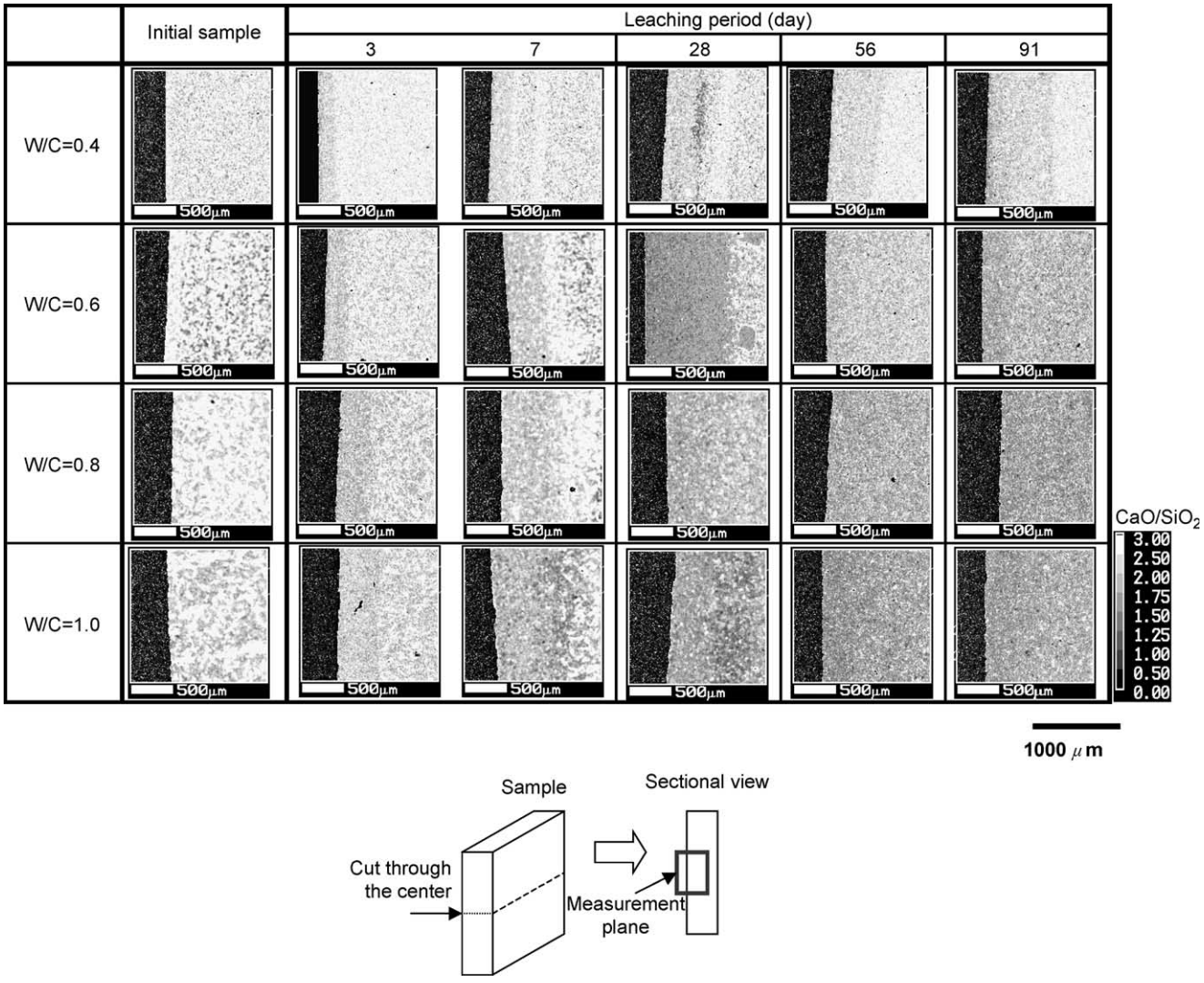

Fig. 10. CaO/SiO_2 molar ratios on the cross-section of the OPC hydrate leached for various leaching times.

data were larger than calculated. It was considered that increments of pore volume were caused not only by the dissolution of $Ca(OH)_2$, but also by the dissolution of another mineral (mainly, C-S-H gel).

3.4. Changes in element distribution in the solid phase

3.4.1. Change in the CaO/SiO_2 ratio along the cross-section of the solid phase

Fig. 10 shows the changes in the element concentration analyzed by EPMA along the cross-section of the samples. They are represented as a CaO/SiO_2 molar ratio (referred to hereafter as the C/S ratio).

After leaching, the C/S ratio in the samples had decreased dramatically in the surface layer, due to the leaching of Ca through the contact surface with the deionized water, while the composition of the initial samples was homogeneous. The inside of the samples after leaching had almost same composition as that of the initial samples. Therefore, the inside, unaltered part and the altered part in the surface layer could be readily distinguished. As an area with a high C/S ratio, indicating the presence of portlandite crystals, was not observed in the altered part, it was thought that the portlandite had leached out completely. As is the case with our studies reported before [14,17,21], the boundary between the unaltered and altered parts observed in this process is referred to as portlandite dissolution front (hereafter the "CH dissolution front").

The CH dissolution front moved inside from the surface with the passage of time, and the movement of the high-W/C sample was faster than that of the low-W/C sample. The CH dissolution front could not be observed clearly in the samples of W/C 0.8 and 1.0 leached for 28 days. Furthermore, the C/S ratio became lower uniformly in the hole part of the sample after being leached for 56 days. In the abovementioned result, the time when the bulk density and the amount of pore increased rapidly was in good agreement with the period when the CH dissolution front was observed, thus, it was judged that the main change of the pore structure was caused by the dissolution of portlandite.

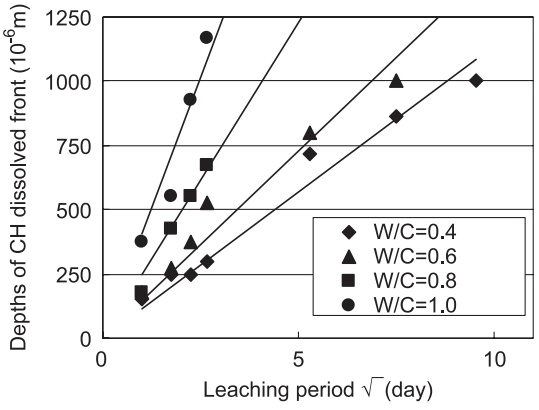

Fig. 11. Depth of the CH dissolved front as a function of the square root of the leaching period.

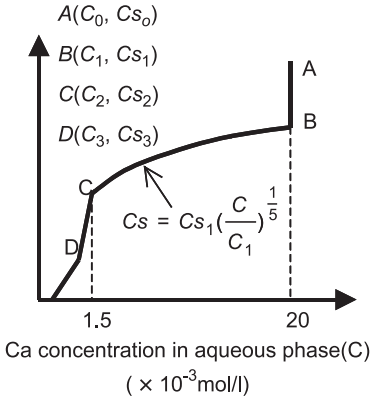

Fig. 12. The curve of the relationship between Ca concentration in the solution and that in the solid used in the model [19].

3.4.2. Movement of the dissolution front

Fig. 11 shows the relationship between the distance from the surface to the CH dissolution front and the square root of the leaching period. A linear relationship was derived by plotting the distance (surface to CH dissolution front) against the square root of the time. This suggests that the transport of Ca, the dissolved component of the portlandite, is by diffusion. Because the slope of the plot was larger as the W/C was larger, it was indicated that the rate of movement of the CH dissolution front was mainly affected by the amount of pore volume.

3.5. Analysis of solid-phase composition

An alteration model [22] that we developed to simulate the progress of the CH dissolution front using the experimental results of leaching tests for hardened alite [21] was used to analyze solid phase composition in the study.

3.5.1. Description of model

3.5.1.1. Basic formula. A basic mass conservation formula for one-dimensional diffusion of Ca in the pore water of hardened cement paste is shown in Eq. (2). The first term on the right side of Eq. (2) represents the diffusion of Ca in the pore water, which is assumed to increase with the increase of porosity associated with dissolution in the model. The second term on the right side represents the dissolution of Ca into the pore water (hereafter referred to as "liquid phase") from the solid phase. Momentarily equilibrium between the solid and liquid phases is assumed in the study, which is shown in Fig. 12.

Coordinates in the model is shown in Fig. 13 [19], where the surface with 10×10 mm is defined as *yz* plane. The diffusion of Ca along the *x* axis can be expressed by Eq. (2),

$$\theta(x,t)\frac{\partial C(x,t)}{\partial t} = D(x,t)\frac{\partial^2 C(x,t)}{\partial x^2} - \frac{\partial C_s(x,t)}{\partial t}, \qquad (2)$$

where t is the time from the start of leaching (s), x is the distance from the edge of the hardened samples (m), $C(x,t)$

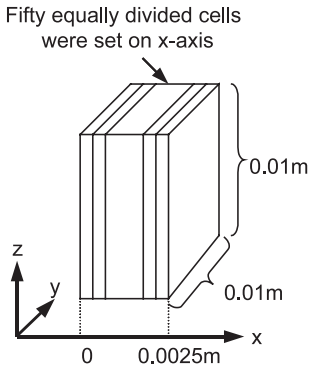

Fig. 13. Coordinates considered in the model [19].

is the Ca concentration in the liquid phase [mol/m^3 (=mmol/l)], $C_s(x,t)$ is the content of Ca (mol/m^3), $\theta(x,t)$ is the porosity (−), and $D(x,t)$ is the effective diffusion coefficient (m^2/s). Fifty equally divided cells with a width of 5×10^{-6} m were set along the direction of the diffusion. Calculation was performed using the finite difference method of finite differences, assuming that Eq. (2) is valid in each cell.

Initial and boundary conditions in the model are shown in Eqs. (3) and (4) respectively,

$$C(x,0) = C_0, \tag{3}$$

$$C(0,t) = C(0.0025,t) = \frac{{}_{total}C(0) - {}_{total}C(t)}{L}, \tag{4}$$

where C_0 is the Ca concentration in the liquid phase at time t (mol/m^3), ${}_{total}C(t)$ is the total quantity of Ca in the hardened cement paste at time t (mol; refer to Eq. (4), and L is the volume of the leaching liquid (m^3). The initial condition, Ca concentration in the liquid phase (=C_0), was set 20 mmol/l, referring to Buil [23]. The boundary conditions, Ca concentrations at x=0 and 0.0025 in the liquid phase, were defined to be the concentrations in the leaching aqueous phase. The concentration in the leaching aqueous phase was calculated from the total quantities of Ca in the hardened cement paste [${}_{total}C(t)$] as shown in Eq. (4).

3.5.1.2. Porosity. Overall porosity determined using MIP was used as the porosity of initial samples. As the experimental data indicated that the increase of porosity obtained by calculation based on the decrease of portlandite, as shown in Fig. 9, is consistent to those obtained in the experiment, the model [22] ignoring the increase due to the dissolution of C-S-H gel was considered to be applicable. Porosities were calculated using Eq. (5) shown below, which was applied in the modeling, taking into consideration the increase of the pore volume associated with the dissolution of portlandite,

$$\theta(x,t) = \theta_0 + \frac{M}{1000d}(\mathrm{CH}_0 - \mathrm{CH}(x,t)), \tag{5}$$

where θ_0 is the porosity of the initial sample (−), M is the molecular weight of portlandite (g/mol), d is the density of portlandite (g/l), CH(x,t) is the quantity of portlandite at the position x at the time t (mol/m^3), and CH_0 is the quantity of portlandite of the initial sample.

3.5.1.3. Diffusion coefficient. The effective diffusion coefficient in porous materials is expressed as Eq. (6) [21].

$$D_e = \frac{\delta}{\tau^2}\theta \times D_f, \tag{6}$$

where δ is the connectivity of pores, τ is the tortuosity (−), and D_f is the diffusion coefficient in free water (m^2/s). The δ and $1/\tau^2$ in the equation are properties anticipated to increase with the increase of the pore volume; however, it will be difficult to determine them independently. Putting $\delta/\tau^2\theta$ as Q in Eq. (7), Q will be increased with the increase of pore volume.

$$Q = \frac{D_e}{D_f} = \frac{\delta}{\tau^2}\theta \tag{7}$$

Q is called "diffusivity" by Atkinson and Nickerson [24] and "relative diffusivity" by Bentz et al. [25]. It is empirically reported that Q is highly correlated to the square value of the porosity for porous rocks, but Atkinson and Nickerson [24] assumed, based on detailed analysis of existing reports, that the effective diffusion coefficients of Cs^+ and I^- in the cement paste are lower than those obtained assuming proportionality to the square value of the porosity, which is interpreted as reflecting the complexity of the pore structure of cementitious materials [24].

Based on these knowledge, considering that the cell width (5×10^{-5} m) in the model is large as compared with capillary pores (1×10^{-5} m or less), diffusion coefficient was determined as Eq. (8). This equation indicates that the diffusion coefficient will be increased with nth power of the ratio of the porosity to the initial sample due to dissolution of portlandite.

$$D(x,t) = \left(\frac{\theta(x,t)}{\theta_0}\right)^n D_0, \tag{8}$$

where n is the parameter and D_0 is the initial diffusion coefficient (m^2/s). The initial diffusion coefficient D_0 was determined considering the porosity of the initial sample and the value of n. The n value was defined as 2 in this study on the basis of preliminary calculation.

3.5.2. Evaluation of CH dissolution front and diffusion coefficient

The experimental results and calculation of the Ca distribution change in the solid phase are shown in Fig. 14, which is a result for the sample with W/C ratio of 0.4. Ca content in the solid sample was expressed as values relative to that of the initial sample. The presence of CH dissolution front and its movement toward the inner side of the sample as the leaching time becomes longer could be reconstructed in the modeling.

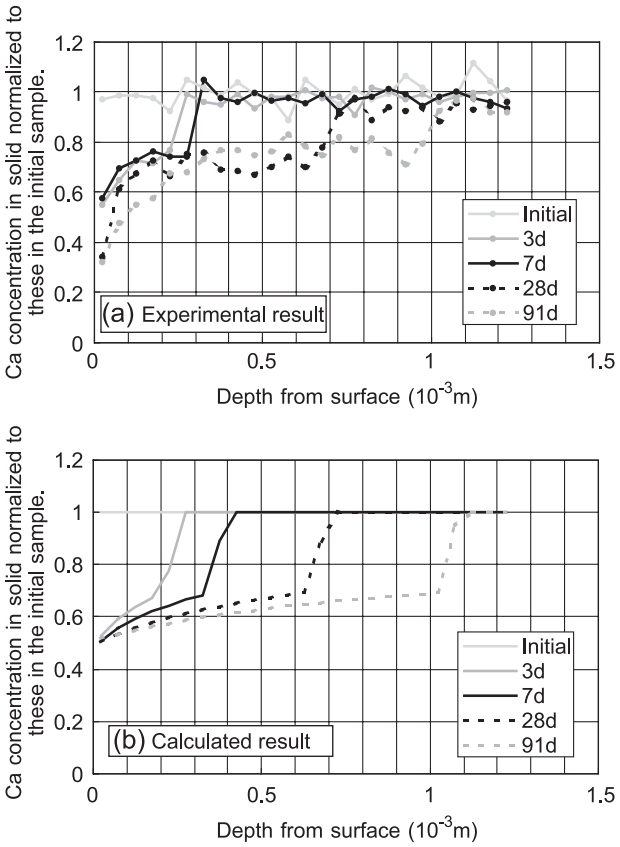

Fig. 14. Ca concentration in the solid normalized to that in the initial sample: (a) experiment, (b) calculation.

Depths of the CH dissolution front in samples are plotted with Ca leached fraction for all W/C ratios in Fig. 15. Leached fraction and the CH dissolution front depth correlate well, and the experimental results and calculation were found to agree well.

The relationship between the calculated effective diffusion coefficient and the porosity is shown in Fig. 16. The

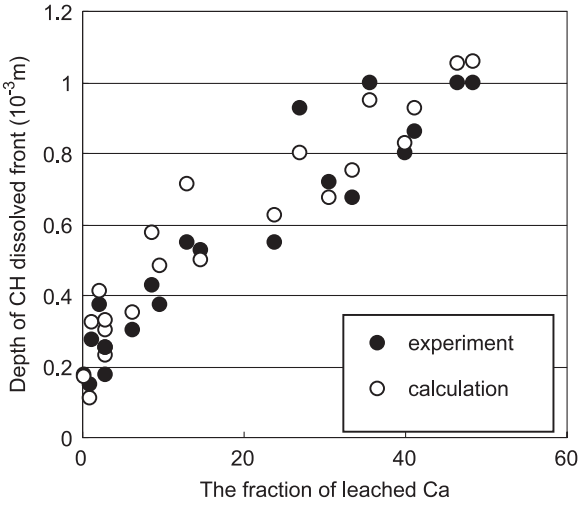

Fig. 15. Depth of the CH dissolved front as a function of the fraction of leached Ca.

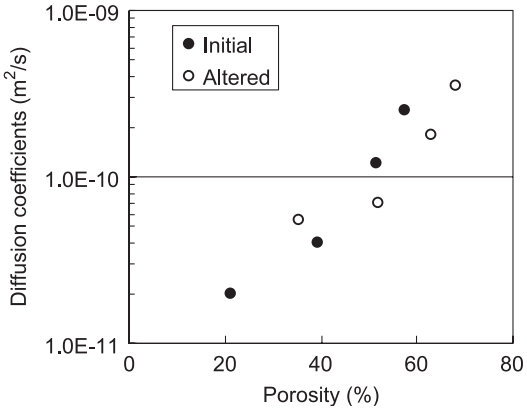

Fig. 16. Porosity dependency of the diffusion coefficient.

diffusion coefficient in the initial sample was determined by fitting the experimental results. As described above, the diffusion coefficient was assumed to be proportional to the square value of the porosity in the applied model [22]. It was found that the calculated effective diffusion coefficients in the unaltered and altered parts show a relatively good correlation with porosity. In the applied model [22], the leaching of both portlandite and C-S-H gel is taken into account for the change in the pore water composition, and the leaching of portlandite, only for the change in the pore volume that affects diffusion. Using this model, the progress of the CH dissolution front for the leaching tests of hardened OPC could be represented, and good correlation between effective diffusion coefficient and porosity was obtained. Consequently, it will be concluded that major leached constituents of hardened OPC will be portlandite and C-S-H gel and that the large pore, which was generated associated with the leaching of portlandite, will significantly affect the diffusion of the leached constituents (Fig. 17).

The relationship between the distance of the CH dissolution front from the surface and the square root of leaching time is also shown in Fig. 15. It indicates that the difference between the calculation and experimental results

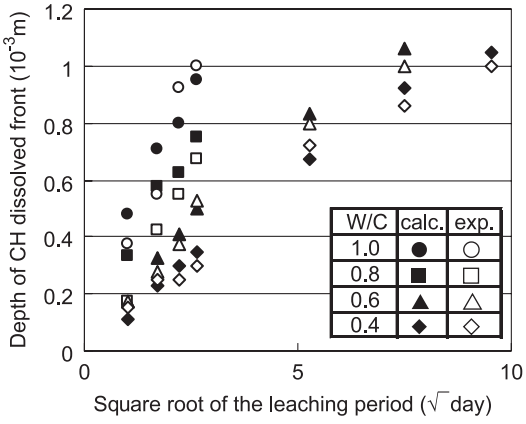

Fig. 17. Depth of the CH dissolved.

becomes larger for samples with larger pore volume. At the comparison of the sample with larger pore volume and that with smaller pore volume, the dissolution amount is larger in the former sample; hence, it is considered that the dissolution amount of C-S-H gel is larger in the former sample, as well as $Ca(OH)_2$. However, at the setting of the diffusion coefficient in this model, the increase of pore volume, accompanied with the dissolution of C-S-H gel, was not considered. Accordingly, differences between the calculation and experimental results are assumed to be due to the effect of C-S-H gel not considered in the change of the diffusion coefficient. For the evaluation of long-term alteration of cementitious material, modeling the leaching of C-S-H gel will be required in the future.

4. Conclusions

We prepared hardened cement paste with variation in pore volume and then leached them in deionized water for a predetermined period. The results, derived from detailed analysis of alteration of hardened cement paste and from evaluation by numerical model, can be summarized as follows:

(1) Portlandite dissolved as the leaching period increased. It was considered that the change in bulk density and pore volume were attributable to the dissolution of portlandite. The larger the pore volume of the samples, the more rapidly portlandite dissolved.
(2) EPMA performed on the cross-sections of the solid phase showed a clear difference between the altered and unaltered parts. The boundary between the two parts was termed the portlandite (CH) dissolution front. As the leaching period became longer, the CH dissolution front shifted towards the inner part of the sample. The time when the bulk density and the amount of pore increased rapidly was in good agreement with the period when the CH dissolution front was observed.
(3) A linear relationship was derived by plotting the distance (surface to CH dissolution front) against the square root of the time. This suggests that the transport of Ca, the dissolved component of the portlandite, is by diffusion.
(4) The dissolution phenomena of hardened OPC was evaluated by the numerical model, with the consideration of two points: one is the increase of pore volume, accompanied with the dissolution of portlandite, and another is the dissolution phenomena of portlandite and C-S-H gel. A basic mass conservation formula for the one-dimensional diffusion of Ca in the pore water of hardened cement paste was used for the evaluation of the CH dissolution front. From the good agreement between experimental results and calculation, it will be concluded that major leached constituents of hardened OPC are portlandite and C-S-H gel, and the large pore, which was generated associated with the leaching of portlandite, will significantly affect the diffusion of leached constituents.

References

[1] S. Tanaka, S. Nagasaki, T. Ooe, M. Hironaga, D. Sugiyama, J. Matsumoto, et al., The role of cement to be expected in radioactive waste disposal system, J. At. Energy Soc. Jpn. 42 (3) (2000) 178–190 (in Japanese).
[2] A. Atkinson, N.M. Everit, R.M. Guppy, Evolution of pH in a radwaste repository, AERER 12594, United Kingdom Atomic Energy Authority, 1987.
[3] A. Atkinson, N.M. Everit, R.M. Guppy, Evolution of pH in a radwaste repository, AERE 12939, United Kingdom Atomic Energy Authority, 1988.
[4] A. Atkinson, R.M. Guppy, Evolution of pH in a radwaste repository, AERE R 12961, United Kingdom Atomic Energy Authority, 1988.
[5] U.R. Berner, Modelling the incongruent dissolution of hydrated cement minerals, Radiochem. Acta 44/35 (1988) 387–393.
[6] P. Faucon, F. Adenot, J.F. Jacquinot, J. Virlet, R. Cabrillac, M. Jorda, Contribution of nuclear magnetic resonance techniques to the study of cement paste water degradation, Proc. of the 10th International Congress on the Chemistry of Cement, 3, Gothenburg, Sweden, 1997, p. 3v003.
[7] P. Faucon, F. Adenot, R. Cabrillac, M. Jorda, Deterioration mechanisms of a cement paste under water attack, concrete under severe conditions 2, in: O.E. Gjorv, K. Sakai, N. Banthia (Eds.), Proceedings of the Second International Conference on Concrete Under Severe Conditions CONSEC'98, vol. 1, Tromso, Norway, 1998, pp. 123–132.
[8] M. Buil, A model of the attack of pure water or undersaturated lime solutions on cement, ASTM STP 1123 (1992) 227–241.
[9] C. Carde, R. Francois, J.M. Torrenti, Leaching of both calcium hydrate and C-S-H from paste: modeling the mechanical behavior, Cem. Concr. Res. 26 (8) (1996) 1257–1268.
[10] F. Adenot, Modeling of the corrosion of the cement paste by deionized water, Cem. Concr. Res. 22 (1992) 489–496.
[11] K. Yokozeki, et al., Concr. Res. Technol. 21 (2) (1999) 961–966 (in Japanese).
[12] M. Toyohara, K. Haga, M. Kaneko, K. Nakata, H. Ueda, H. Nogiwa, Modeling a cement alteration by coupling dissolution of hydrates and mass transport, Trans. At. Energy Soc. Jpn. 1 (2) (2002) 134–143 (in Japanese).
[13] K. Haga, M. Shibata, K. Okada, M. Hironaga, S. Tanaka, S. Nagasaki, $(SiO_4)^{4-}$ structure change in C-S-H on dissolution processes of tricalcium silicate hydrate, J. Nucl. Fuel Cycle Environ. 5 (2) (1999) 43–50 (in Japanese).
[14] K. Haga, M. Hironaga, S. Tanaka, H. Uchikawa, Reaction and compositional and structural change of hardened C_3S paste in the process of dissolution, Cem. Sci. Concr. Technol. 53 (1999) 36–43 (in Japanese).
[15] K. Haga, M. Shibata, Y. Fukaya, Y. Kobayashi, M. Imamura, Alteration test of hydrated cement paste by water permeation using centrifugal force, J. Nucl. Fuel Cycle Environ. 6 (2) (2000) 167–173 (in Japanese).
[16] K. Haga, M. Shibata, M. Hironaga, S. Tanaka, S. Nagasaki, Silicate anion structural change in calcium silicate hydrate gel on dissolution of hydrated cement, J. Nucl. Sci. 5 (2002) 540–547.
[17] K. Haga, M. Shibata, M. Hironaga, S. Tanaka, S. Nagasaki, Pore structural and compositional change in hardened cement paste in the process of dissolution, Cem. Concr. Res. (submitted).

[18] P. Faucon, F. Adenot, M. Jorda, R. Cabrillac, Behavior of crystallized phases of portland cement upon water attack, Mat. Struct. 30 (1997) 480–485.
[19] M. Daimon, S.A. Abo-El-Enein, G. Hosaka, S. Goto, R. Kondo, Pore structure of calcium silicate hydrate in hydrated tricalcium silicate, J. Am. Ceram. Soc. 60 (3–4) (1977) 110–114.
[20] H.F.W. Taylor, Cement Chemistry, 2nd ed., Thomas Telford Services, Academic Press, London, 1997.
[21] K. Haga, S. Sutou, M. Hironaga, S. Tanaka, S. Nagasaki, Study on the leaching behavior of Ca from the alite hydrate, J. Mater. Concr. Struct. Pavement, JSCE (in Japanese) (submitted).
[22] S. Sutou, K. Haga, M. Hironaga, S. Tanaka, S. Nagasaki, Modelling the leaching behavior of Ca and the dependence of porosity on the diffusion coefficient, J. Mater. Concr. Struct. Pavement, JSCE (in Japanese) (submitted).
[23] M. Buil, A model of the attack of pure water or undersaturated lime solutions on cement, ASTM STP 1123 (1992) 227–241.
[24] A. Atkinson, A.K. Nickerson, The diffusion of ions through water-saturated cement, J. Mater. Sci. 19 (1984) 3068–3078.
[25] D.P. Bentz, D.B. Gingold, E.J. Garboczi, C.J. Lobb, H.M. Jennings, Diffusion studies in a digital-image-based cement paste microstructural model, in: S. Mindess (Ed.), Advances in Cementitious Materials, Ceramic Transactions, vol. 16, American Ceramics Society, Westerville, Ohio, 1991, p. 211.